SHADOW REGION IMAGING ALGORITHM USING ARRAY ANTENNA BASED ON APERTURE SYNTHESIS OF MULTIPLE SCATTERED WAVES FOR UWB RADARS

Shouhei Kidera

Graduate School of Informatics and Engineering, University of Electro-Communications, Tokyo, Japan
Email: kidera@ee.uec.ac.jp

ABSTRACT

Ultra-wide band (UWB) pulse radar has a definite advantage over optical ranging techniques, as to applicablity to the harsh optical environment, such as the dark smog, or strong backlight. We have already propoposed the extended Synthetic Aperture Radar (SAR) algorithm employing the multiple scattered waves, which aims at enhancing the reconstructible region of the target boundary including the shadow. However, it still suffers from the shadow region in the case of the target with a sharp inclination or deep concave boundary, because it assumes the antenna scanning whose real aperture size is too small. To resolve this difficulty, this paper proposes an extension algorithm using the array antenna model. While this extension is quite simple, the effectiveness of the proposed method is nontrivial regarding to the expansion of the imaging range. The results from numerical simulations verify that our method remarkably enhances the visible range of target surfaces without *a priori* knowledge of target shapes or a preliminary observation of its surroundings.

Index Terms— UWB radars, Multiple scattered waves, SAR, Shadow region imaging, Array antennas, Complex-shaped or multiple targets

1. INTRODUCTION

UWB radar with high range resolution creates various applications for near field sensing. It is applicable to non-contact measurement such as reflector antennas or aircraft bodies that have high-precision and specular surfaces, or spatial measurement for rescue or resource exploration robots that can identify a human body or materials even in darkness, smog or high-concentration gas. It is also applicable to non-contact spatial measurement of industrial products with high-precision or specular surfaces, such as reflector antennas or aircraft bodies. Moreover, it is promising for intruder detection or elderly care in a private room, whereas an optical camera generates an unavoidable problem of invasion of privacy.

Various kinds of radar algorithms have been developed aimed at geosurface measurement, landmine detection, non-destructive testing or indoor sensing, based on aperture synthesis or range migration [1, 2]. Time reversal methods have been extensively developed for target detection in cluttered situations [3], or for super-resolution imaging by incorporating the MUSIC (Multiple Signal Classification) algorithm [4]. Different approaches aiming at clear boundary extraction are also promising for real-time and super-resolution radar imaging, by using the reversible transform BST (Boundary Scattering Transform) between the range wavefront and the target boundary [5], calculating the envelope of spheres determined by the observed ranges [6] or directly reconstructing a complex-shaped target boundary using range points migration [7]. However, they all have the inherent problem that the baseline length theoretically limits the reconstructible range of radar imagery. In many cases, the greater part of the target shape, such as the side of target, falls into a shadow region, which is never reconstructed since only the single scattered components are used for imaging.

To overcome this problem, we have already proposed the imaging algorithm called multiple scattered SAR [8]. This is based on the principle that a multiple scattered signal includes additional independent information on the target points compared with information from a single scattered signal. In making use of the multiple scattered waves, this method significantly enhances the imagery range, including the region regarded as a shadow in the original SAR [1]. Furthermore, this method does not require a priori information of surroundings or target modeling, which is necessary for other techniques using multiple scattered waves [9].

It has been demonstrated that while the former work enhanced the imagery range for several target cases, the greater part of the target boundary still falls into a shadow, even when using the multiple scattering waves. This is because an antenna scanning observation is assumed for which the real aperture size often becomes insufficient to recognize a target shape, especially if it has a deep-set concave shape or a sharply-inclined boundary. For this difficulty, this paper introduces an observation model using array antenna, where the real aperture size is significantly enhanced. While this extension is quite simple, the proposed model greatly enhances the imagery range, despite the fact that the baseline of the antenna is the same as that in the antenna scanning model. The numerical simulation proves that the imagery range using the

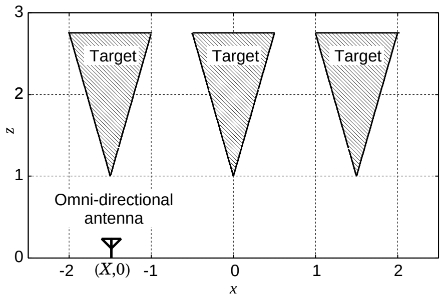

Fig. 1. System model.

array antenna model expresses the target shape, which was never recognized by the former model.

2. SYSTEM MODEL

Fig. 1 illustrates the system model, where it assumes the 2-dimensional problem and TE mode waves, for simplicity. It also presumes that the target has high conductivity such as a metal,and an arbitrary shape with a clear boundary. The propagation speed of the radio wave c is assumed to be known constant. An omni-directional antenna is used, and the transmitting current is given by a mono-cycle pulse. The real space in which the target and antenna are located is expressed by the parameters $\boldsymbol{r} = (x, z)$, which are normalized by λ, the central wavelength of the pulse.

3. CONVENTIONAL MODEL FOR MULTIPLE SCATTERED SAR

The extended SAR algorithm using the double scattered signals has already been developed to enhance the imagery range, which becomes a shadow in the original SAR image [8]. This method assumes that a mono-static antenna is scanned along the x axis, and $s(X, Z)$ is defined as the output of the Wiener filter at the antenna location $(X, 0)$, where $Z = \mathrm{c}t/(2\lambda)$ is expressed by the time t. The procedure creating $s(X, Z)$ is detailed in [7]. This method is based on the simple principle that, “a double scattered wave propagates a different path from that of a single scattered one, and this wave often includes significant information on two reflection points on the target boundaries”. The suitable use of multiple scattered signals is promising as shadow region imaging. It calculates the image migrated by double scattered signals as

$$\begin{aligned} I_2^{\mathrm{S}}(\boldsymbol{r}) \;&=\; -\int_{\boldsymbol{r'} \in R} \int_{X \in \Gamma} I_1^{\mathrm{S}}(\boldsymbol{r'}) \\ &\quad \cdot s\left(X, d(\boldsymbol{r}, \boldsymbol{r'}, X, X)/2\right) \mathrm{d}X \mathrm{d}x' \mathrm{d}z', \qquad (1) \end{aligned}$$

where Γ is the scanning range of the antenna, $\boldsymbol{r'} = (x', z')$ is defined, R is the region of the real space, and $d\left(\boldsymbol{r}, \boldsymbol{r'}, X, X'\right) = \sqrt{(x - X)^2 + z^2} + \sqrt{(x' - X')^2 + z'^2} + \sqrt{(x - x')^2 + (z - z')^2}$ holds. The minus sign of the right term in Eq. (1) creates a positive image focused by double scattered waves, that have an anti-phase relationship compared with single scattered waves. The initial image $I_1^{\mathrm{S}}(\boldsymbol{r})$ is defined as the original SAR image as

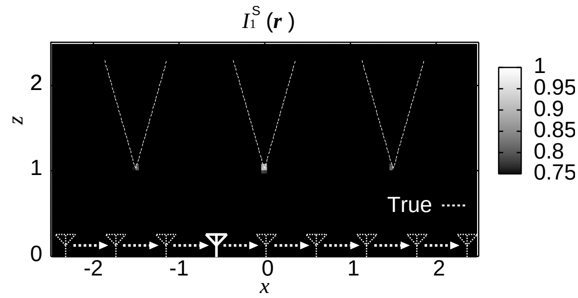

Fig. 2. Estimated image $I_1^{\mathrm{S}}(\boldsymbol{r})$, where antenna scanning model is assumed.

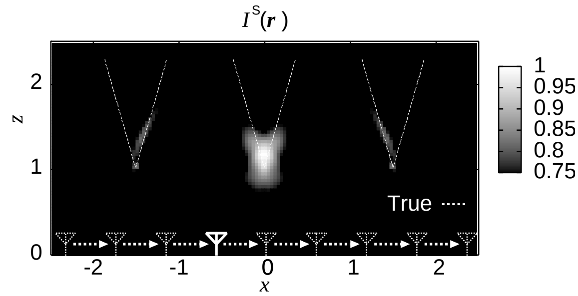

Fig. 3. Estimated image $I^{\mathrm{S}}(\boldsymbol{r})$, where antenna scanning model is assumed.

$$I_1^{\mathrm{S}}(\boldsymbol{r}) = \int_{X \in \Gamma} s\left(X, d(\boldsymbol{r}, \boldsymbol{r}, X, X)/2\right) \mathrm{d}X, \qquad (2)$$

Eq. (1) expresses the aperture synthesis of the received signals by considering only a double scattered path. The final image is defined as

$$I^{\mathrm{S}}(\boldsymbol{r}) = \frac{I_1^{\mathrm{S}}(\boldsymbol{r}) H(I_1^{\mathrm{S}}(\boldsymbol{r}))}{\max_{\boldsymbol{r}} I_1^{\mathrm{S}}(\boldsymbol{r})} + \frac{I_2^{\mathrm{S}}(\boldsymbol{r}) H(I_2^{\mathrm{S}}(\boldsymbol{r}))}{\max_{\boldsymbol{r}} I_2^{\mathrm{S}}(\boldsymbol{r})} \qquad (3)$$

where $H(*)$ is the Heaviside function. This method directly enhances the imagery range with only a single observation, and does not require any priori information on surroundings, or target modeling, which are substantial advantages for the other algorithms [9].

An example of this method is presented as follows. The received signals are calculated by the FDTD method, and obtained at 401 locations in the range, $-2.5 \leq X \leq 2.5$. The target boundary is assumed as shown in Fig. 1. Figs. 2 and 3 show $I_1^{\mathrm{S}}(\boldsymbol{r})$ and $I^{\mathrm{S}}(\boldsymbol{r})$, respectively. Each image is normalized by its maximum value. $I_1^{\mathrm{S}}(\boldsymbol{r})$ expresses only the convex

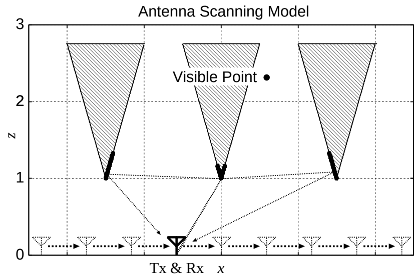

Fig. 4. Visible points with double scattered waves in antenna scanning model.

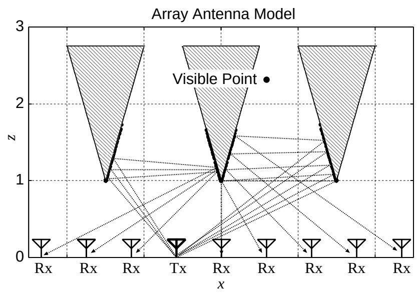

Fig. 5. Visible points with double scattered waves in array antenna model.

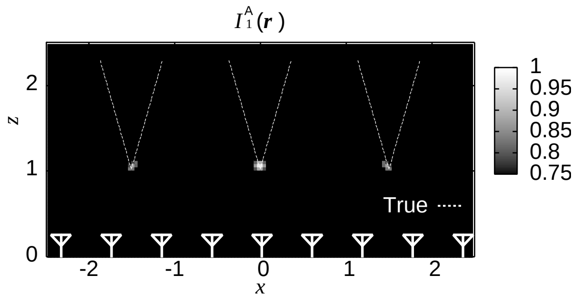

Fig. 6. $I_1^{\mathrm{A}}(\boldsymbol{r})$ in array antenna model.

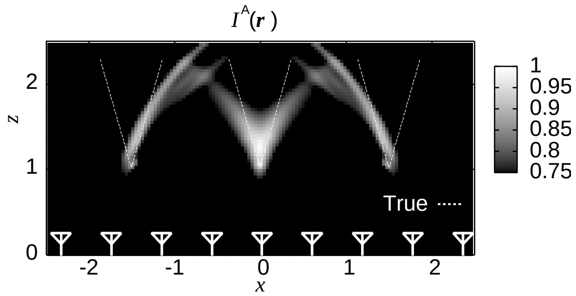

Fig. 7. $I^{\mathrm{A}}(\boldsymbol{r})$ in array antenna model.

edges of the triangle boundary because only single scattered signals are used for imaging. In addition, Fig. 3 shows that the triangle side of the target is still not reconstructed, despite the use of double scattered waves. This is because the double scattered signals, that propagate through the sharp inclined side of the triangles, are not observed for any antenna location. The above result suggests that, to enhance the range of the radar imagery, a large real aperture size is necessary.

4. PROPOSED MODEL FOR MULTIPLE SCATTERED SAR

To outperform the former algorithm, we propose to use the array antenna model for the multiple scattered SAR, which can enhance a real aperture size. Figs. 4 and 5 show the visible points in the use of antenna scanning and array antenna models, respectively. The numbers of scanning samples or array antenna are 26 for $-2.5 \leq x \leq 2.5$, whose combination number as ${}_{26}\mathrm{C}_2 = 325$ is less than the number of samples in scanning model as 401. Each visible point is calculated using the geometrical optics, considering that the propagation path is secluded from other targets. In the scanning model as shown in Fig. 4, there are a few points around the lower side of triangle boundaries, but the most of the visible points are concentrated on the edges. It is confirmed that the locations of these points are focused on the same region, even if the number of scanning sample increases. Conversely, in the array antenna model, the number of the visible points around each triangle's side remarkably increases, and the central target shape can be identified as the part of triangle, despite an aperture size that is equivalent to the aperture in the previous model. This is because the combination of the transmitting and receiving antennas creates different scattering paths, and increases the number of independent target points. This reveals that the extension for the array model offers a substantial improvement, and it is a unique characteristic for the multiple scattered signals.

Here, the transmitting and receiving antenna locations are defined as $(X_{\mathrm{T}}, 0)$ and $(X_{\mathrm{R}}, 0)$, respectively. In each combination of X_{T} and X_{R}, the output of the Wiener filter is obtained as $s(X_{\mathrm{T}}, X_{\mathrm{R}}, Z)$. The previous work is readily extended to the bi-static model, and the estimated image with the array antenna model $I_2^{\mathrm{A}}(\boldsymbol{r})$ is calculated as,

$$I_2^{\mathrm{A}}(\boldsymbol{r}) = -\int_{\boldsymbol{r'} \in R} \int_{X_{\mathrm{R}} \in \Gamma} \int_{X_{\mathrm{T}} \in \Gamma} I_1^{\mathrm{A}}(\boldsymbol{r'}) \cdot s\left(X_{\mathrm{T}}, X_{\mathrm{R}}, d(\boldsymbol{r}, \boldsymbol{r'}, X_{\mathrm{T}}, X_{\mathrm{R}})/2\right) \mathrm{d}X_{\mathrm{T}} \mathrm{d}X_{\mathrm{R}} \mathrm{d}x' \mathrm{d}z', \quad (4)$$

where $I_1^{\mathrm{A}}(\boldsymbol{r})$ is defined as,

$$I_1^{\mathrm{A}}(\boldsymbol{r}) = \int_{X_{\mathrm{T}} \in \Gamma} \int_{X_{\mathrm{R}} \in \Gamma} s\left(X_{\mathrm{T}}, X_{\mathrm{R}}, d(\boldsymbol{r}, \boldsymbol{r}, X_{\mathrm{T}}, X_{\mathrm{R}})/2\right) \cdot \mathrm{d}X_{\mathrm{R}} \mathrm{d}X_{\mathrm{T}}. \quad (5)$$

The final image is similarly defined as in Eq. (3). This array model significantly enhances the real aperture size. That is,

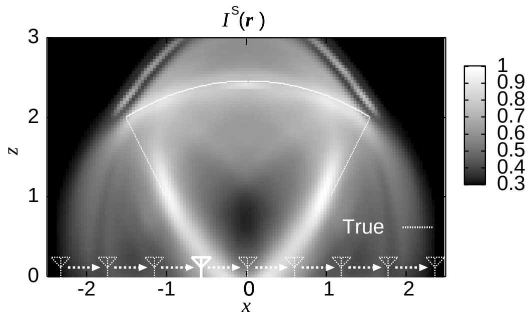

Fig. 8. $I^{\mathrm{S}}(\boldsymbol{r})$ in antenna scanning model for the concave target.

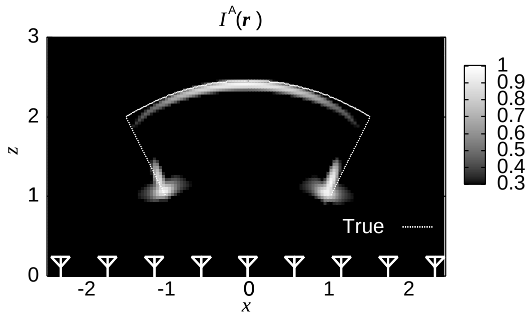

Fig. 9. $I^{\mathrm{A}}(\boldsymbol{r})$ in array antenna model for the concave target.

it expands a visible range in spite of the fact that the baseline lengths of both the conventional and proposed models are the same.

5. PERFORMANCE EVALUATION

This section presents the example used in the proposed model. Figs. 6 and 7 show $I_1^{\mathrm{A}}(\boldsymbol{r})$ and $I^{\mathrm{A}}(\boldsymbol{r})$ for the triangular objects, respectively. The number of data samples is the same as in array antenna is 26, assuming the same baseline as in Fig. 2. Fig. 6 indicates that the image obtained by single scattered SAR $I_1^{\mathrm{A}}(\boldsymbol{r})$ does not enhance the imagery range, entirely, even if the real aperture size is enhanced. This is because it uses only the single scattered wave for imaging. On the contrary, Fig. 7 reveals that the triangular side of the target is reconstructed, and offers a substantial image identifying the triangular shapes. This is because the array observation increases the number of double scattered signals, which includes independent information on the target boundary, thus the enhanced real aperture size improves the imagery range.

Additional examples for a concave boundary target are investigated as follows. Figs. 8 and 9 show $I^{\mathrm{S}}(\boldsymbol{r})$ and $I^{\mathrm{A}}(\boldsymbol{r})$ for the trapezoidal objects, respectively. As shown in Fig. 8, there are many false images far from the actual target boundary because the received signals from the side of target cannot be observed in any antenna location in this model. Contrarily, the image obtained by the proposed model in Fig. 9 enhances the visible range of the side of the target, while the false images are effectively suppressed.

It confirms that the image obtained by the proposed method remains accurate in a noisy situation, where the S/N of the double scattered signal is higher than 20 dB. In addition, this method requires the quadruple integration of the received signals in Eq. (4), which requires about 20 minutes for the calculation using a Intel Pentium D 2.8 GHz processor. Thus an acceleration in the imaging speed is also required to use the extended method for 3-dimensional problems.

6. CONCLUSION

This paper proposed a shadow imaging algorithm based on aperture synthesis of double scattered waves using an array antenna model. The previous work is extended to the array antenna observation, where a bi-static model of the multiple scattered SAR is introduced. Although this extension is simple and not novel in itself, the imagery range is substantially improved with the larger real aperture size, especially when using the multiple scattered SAR method. The result of the numerical simulation successfully proves that the proposed model makes shadow region visible for one of the most difficult target cases, despite the fact that the baseline length is the same for both conventional and proposed models.

7. REFERENCES

[1] W. M. Brown, *IEEE Trans. Aerosp. Electron. Syst.*, vol. AES–3, pp. 217–229, Mar. 1967.

[2] J. Song et al., *IEEE Trans. Geosci. Remote Sens.*, vol.44, no.6, pp. 1462–1469, Jun, 2006.

[3] D. Liu et al., *IEEE Trans. Antenna Propagat.*, vol. 53, no. 9, pp. 3058–3066, Sep, 2005.

[4] E. A. Marengo, F. K. Gruber and F. Simonetti, *IEEE Trans. on Image Processing*, vol. 16, no. 8, pp. 1967–1984, Aug, 2007.

[5] T. Sakamoto and T. Sato, *IEICE Trans. Commun.*, vol.E87-B, no.5, pp. 1357–1365, 2004.

[6] S. Kidera, T. Sakamoto and T. Sato, *IEEE Trans. Geosci. Remote Sens.*, vol. 46, pp. 3503–3513, no. 11, Nov, 2008.

[7] S. Kidera, T. Sakamoto and T. Sato, *IEEE Trans. Geosci. Remote Sens.*, vol. 48, no. 4, pp. 1993-2004, Apr., 2010.

[8] S. Kidera, T. Sakamoto and T. Sato, *Proc. of PIERS 2009.*, Vol. 5, No. 4, pp. 393–396, Aug, 2009.

[9] J. M. F. Moura, and Y. Jin, *IEEE Trans. on Signal Process.*, vol. 55, no. 1, pp. 187–201, Jan, 2007.